Contents lists available at ScienceDirect

Petroleum Science

journal homepage: www.keaipublishing.com/en/journals/petroleum-science



Original Paper

Measurement while drilling of downhole engineering parameters by application of a newly designed micro-measurer



Yu-Xi Wang ^{a, b}, Mu Li ^{c, d}, Mao-Lin Liao ^{a, b, *}, Wei Liu ^c, Ting-Rui Li ^{a, b}, Joseph Páez Chávez ^{e, f}, Gong-Hui Liu ^g, Jun Li ^d, Sheng-Lian Yao ^h

- ^a School of Mechanical Engineering, University of Science and Technology Beijing, Beijing, 100083, China
- ^b Downhole Intelligent Cybernetics Institute, University of Science and Technology Beijing, Beijing, 100083, China
- ^c CNPC Engineering Technology R&D Company Limited, Beijing, 102206, China
- ^d School of Petroleum Engineering, China University of Petroleum (Beijing), Beijing, 102249, China
- e Center for Applied Dynamical Systems and Computational Methods (CADSCOM), Faculty of Natural Sciences and Mathematics, Escuela Superior Polit'ecnica del Litoral, P.O. Box 09-01-5863, Guayaguil, Ecuador
- f Center for Dynamics, Department of Mathematics, TU Dresden, Dresden, D-01062, Germany
- g School of Mechanical and Energy Engineering, Beijing University of Technology, Beijing, 100124, China
- ^h School of Materials Science and Engineering, University of Science and Technology Beijing, Beijing, 100083, China

ARTICLE INFO

Article history: Received 4 March 2024 Received in revised form 24 April 2025 Accepted 24 April 2025 Available online 30 April 2025

Edited by Jia-Jia Fei

Keywords: Measurement of temperature and pressure profiles MEMS sensor Time-depth conversion Downhole internet of things

ABSTRACT

As the well drilling depth has broken through the 10,000 m in China, accurate measurements of downhole engineering parameters, such as annulus temperature and pressure for the whole wellbore, are significant in controlling potential downhole complexities. In this present work, a new micromeasurer is developed by integrating measurements of downhole temperature, pressure, magnetic field strength, and its own dynamic signals. The micro-measurer can flow with drilling fluid from the drillstring to the bottomhole and then float up back to the ground via the wellbore annulus. Compared with other downhole measurement tools that are fixedly connected to the drill string, its "measure-andmove-on" approach reduces the residence time in the high-temperature and high-pressure zone at the bottomhole; moreover, both the pressure and temperature at different well depth can be measured, thereby the temperature and pressure profiles of the whole wellbore can be constructed. In addition, the bluetooth low energy (BLE) technique is applied to offer the micro-measurer with the capability of wireless information transmission; while hydrodynamic optimization of the micro-measurer is carried out to design the structure of the micro-measurer, which can promote its recovery rate from downhole. In addition, an intelligent joint for releasing micro-measurers from the wellbore annulus is also proposed, aiming to overcome the limitation imposed by the nozzle on the size of the micro-measurer. Both the indoor experiments and the field tests have verified the feasibility of the newly designed micromeasurer, which is a key step for establishing a complete downhole internet of things (IoT) system to serve the intelligent drilling in the future.

© 2025 The Authors. Publishing services by Elsevier B.V. on behalf of KeAi Communications Co. Ltd. This is an open access article under the CC BY-NC-ND license (http://creativecommons.org/licenses/by-nc-nd/

4.0/)

1. Introduction

As oil-gas exploration progressively transitions from middleshallow to deep reservoirs, the fracture behaviors in the deep zone, along with elevated temperatures and pressures, combined

* Corresponding author.

E-mail address: liaomaolin@ustb.edu.cn (M.-L. Liao).

Peer review under the responsibility of China University of Petroleum (Beijing).

with the narrow safety density window of drilling fluids, escalate the probability of downhole anomalies. These anomalies, such as overflow and mud loss, can lead to complex situations, including collapse and blowout, resulting in both economic losses and potential casualties (An et al., 2023; Suo et al., 2023; Zhang et al., 2023, 2024). Consequently, there is a critical need for a distributed measurement system of temperature and pressure profiles for the whole wellbore to achieve a comprehensive analysis and evaluation of downhole conditions.

The evolution from single-point, dual-point measurement to measurement of physical parameters profiles represents a prevailing trend in the advancement of logging tools. Dual-point measurement research initiated earlier. In 2015, Baker Hughes invested in a study on the impact of the positions of two combinational pressure sensors on the quality of continuous wave mud pulse detection (Emmerich et al., 2015). Yan et al. (2019) delved into the denoising principle using the dual-pressure-sensor timedomain delay differential method, identifying a 20 m interval as the optimal solution of dual-sensor installation. Wang et al. (2020, 2023) applied dual-point pressure and flow sensors, combined with neural network algorithms and a genetic algorithm-based model to detect well gas kick, achieving accurate gas fraction determination. Gutierrez et al. (2021) established a dual-point measurement system by adding a secondary directional sensor to an existing measurement-while-drilling (MWD) tools, conducting field tests on nine wells, and confirming the advantages of the dualpoint measurement system in positioning accuracy. For constructing downhole physical parameters profiles, distributed fiber-optic sensing (DFOS), encompassing distributed temperature sensing (DTS), distributed strain sensing (DSS), and distributed acoustic sensing (DAS), was developed (Sun et al., 2021). Hemink and van der Horst (2018) utilized DTS to detect thermal effects from lift gas flow, and DAS to identify gas flow through acoustic measurements, providing deeper insights into wellbore circumstance and enhancing decision-making in gas lift operations. Gurjao et al. (2021) researched on a forward modeling approach using both analytical and numerical solutions to generate DSS/DAS synthetic data, captured relevant phenomenon associated with hydraulic and natural fractures interaction. He et al. (2022) developed a quasidistributed temperature and pressure sensing system using fiberbased Fabry-Perot Interferometer (FPI) pressure sensor in conjunction with Fiber Bragg Grating (FBG) temperature sensor array, successful applying during the second gas hydrate trial production in the South China Sea. While quasi-distributed downhole temperature and pressure measurement systems have been successfully developed and validated, achieving measurements of temperature and pressure profiles for the entire wellbore remains a challenging task, difficult to attain with conventional methods.

MEMS technology emerges as a viable solution to address challenges by seamlessly integrating miniaturized mechanical and electronic components, particularly in the context of large-scale distributed measurement systems (Liu et al., 2022). Wang et al. (2018) harnessed a Reduced Inertial Sensor System (RISS), comprising MEMS gyroscope and three-axis MEMS accelerometers, to deliver a 3D navigation solution for continuous wellbore surveying. This approach presents a robust and efficient alternative to traditional methods in directional drilling. Li et al. (2023b) expanded Wang's work by incorporating a MEMS magnetometer and an odometer, devising a multi-sensor fusion-based 3D trajectory measurement algorithm for underground pipelines. In a similar way, van Pol et al. (2018) conceptualized "Pipers", a miniature measuring tool based on MEMS. Pipers is equipped with an inertia sensor, a magnetometer, a combined pressure and temperature sensor, and an advanced acoustic leak detection system. Notably, in 2021, Pipers clinched the "Spotlight on New Technology" award at the International Offshore Oil and Gas Technology Conference (OTC), underscoring the far-reaching application potential of MEMS technology in oil and gas well engineering.

Through the collaborative efforts of Saudi Aramco and the University of Tulsa, a pioneering measurement technique based on MEMS have been proposed for constructing wellbore temperature profiles. Along these lines, Yu et al. (2012) introduced the initial research on this downhole microsphere chip measurement tool, naming it "microchip". Comprising MEMS sensors, a kernel circuit

system, and chemical protective coatings, microchip demonstrated the ability to flow as circulation of drilling fluid, measuring and recording downhole temperature and pressure. Subsequently, various oilfield service company and research institutions have delved deeper into this technology (Liu et al., 2023; Zhu et al., 2021). Li et al. (2017, 2020) conducted field tests in wells up to a depth of 2820 m, resulting in a 36% physical recovery rate and a 24% data recovery rate. They also introduced an iterative method for correlating measured time-series data with drilling depth. To address electric leakage risks of the microchip during wire communication with upper computer, Shi et al. (2020) applied electromagnetic coils for wireless charging and initialization. Dokhani et al. (2022) modified the transient thermal model based on the temperature data from the microchip, validating it through field test in two wells, showing a close match between the predicted return mud temperature and the measured temperature data

The development of a similar measurement tool called the "micro-measurer" by Li et al. (2023a) involved optimizing space utilization through the design of a rigid-flexible printed circuit board (PCB) to integrate temperature, pressure, magnetic and inertial sensors. This technique also offers an additional data transmission path for existing logging-while-drilling (LWD) tools, enhancing data transmission efficiency. In a related development, Li et al. (2022) introduced microchip-storage-balls (MSBs) to establish a time-division multiplexing data transmission system. MSBs can be released directly from the drill collar into the annulus via a release pushrod, flowing as circulation of drilling fluid and eventually recovered to transmit data from LWD tools. While numerous studies have showcased the significance of MEMS-based micro measurement devices as a breakthrough in constructing downhole physical parameter profiles, challenges persist.

Current micro measurement devices rely on wired serial connections for data transmission, introducing the risk of data loss in the event of recovery operations failures or damage to the exposed data interface. The flow as circulation of drilling fluid, which includes flowing out of the nozzle and floating up in the annulus, presents a dilemma between density and volume. In deeper wells, the increased circulation time of drilling fluid reduces the timeliness of the measurement data. Additionally, impacts in the vicinity of the bit while drilling have the potential to damage protective coatings, consequently lowering the recovery rate. There is a need for the development of reliable techniques to recover the micro measurement device from vibrating screen or mud pit.

In this research, we have developed both a new generation of micro-measurer and an intelligent joint for releasing micromeasurers to address existing shortcomings. The key contributions in this research are outlined as follows:

- (1) The new generation of micro-measurer integrates the measurements of temperature, pressure, and dynamic signals. Based on the application of Computational Fluid Dynamics (CFD) software Fluent, the structure design with optimal hydrodynamic properties for the micro-measurer is carried out to enhance the recovery rate of the micro-measurer when it works in complex downhole environment. The energy-friendly Bluetooth Low Energy (BLE) 5.2 network is applied to promote the wireless communication and control of the micro-measurer.
- (2) In order to conduct the laboratory hydrodynamic test of the micro-measurer, we have constructed an L-shaped pipe-inpipe device with pipe diameters to mimic the real horizontal well. Based on this experimental rig, two time-depth conversion methods, for correlating measured time-series data with drilling depth have verified, which can be

applied to construct the temperature and pressure profile for wellbore.

(3) Two types of controllable releasing structures for downhole intelligent joint are proposed, whose purpose is to enhance the stability and intelligence of the distributed downhole measurement system, paving the way for the establishment of a complete downhole IoT system in the future.

2. Design of micro-measurer

The development of a micro-measurer includes kernel system design, structure optimization, pouring, and molding. Particularly, a micro-measurer will integrate circuit board, MEMS sensors and micro-power supply unit within a remarkably compact volume of just 0.654 cm³.

2.1. Design of kernel circuit system

As the micro-measurer will flow with drilling fluid for over 5 h in downhole, and also needs to pass through the nozzle of drill bit, the kernel circuit should be designed to be compact and energy-efficient. For the collaborative measurement of multiple wellbore physical parameters, a variety of MEMS components are integrated into the micro-measurer:

- (1) A fine-line K-type thermocouple temperature sensor is used for measuring temperature with a range of -40 to $200\,^{\circ}$ C and the accuracy of $+0.1\,^{\circ}$ C.
- (2) A nano-film pressure sensor is used for measuring downhole pressure with a range of 0–200 MPa and the accuracy of 0.2 MPa
- (3) A high-precision six-axis Inertial Measurement Unit (IMU) is applied for measuring the vibration condition of the micromeasurer with acceleration up to 16 g, angular rate up to 2000 dps and the resolution of 16 bits.
- (4) A three-axis magnetometer is applied for measuring the magnetic field strength in the downhole environment up to 1600 μT. The magnetometer can assist in time-depth conversion by capturing the peak values when the micromeasurer passing magnetic rings.
- (5) A 8 Mbit serial flash with dual output is applied for the measured data storage.

The schematic of the kernel system is depicted in Fig. 1.

The MEMS components are seamlessly incorporated into a six-layer buried and blind via PCB (with a minimum diameter of 7.5 mm), ensuring strict adherence to size limitations, as shown in Fig. 2. The micro-measurer stands out from other micro measurement devices due to its wireless capabilities enabled by a Wireless Microcontroller Unit (MCU). It features a 76.8 MHz Cortex-M33 processor and a high-performance 2.4 GHz radio, facilitating energy-friendly BLE networking. This simplifies wireless activation, data transmission, and contributes to the recovery process (Hancke and Silva, 2021).

The micro-sized, highly energy-efficient design of the kernel system ensures that the operating current of the micro-measurer below 3 mA, with sleep current reaching microampere (μ A) levels. With a micro-power supply unit boasting a capacity of 53 mAh, the micro-measurer can theoretically operate for over 15 h.

2.2. Structure optimization

Hydrodynamic properties of a micro-measurer, directly influenced by its structure design, are crucial for circulation and

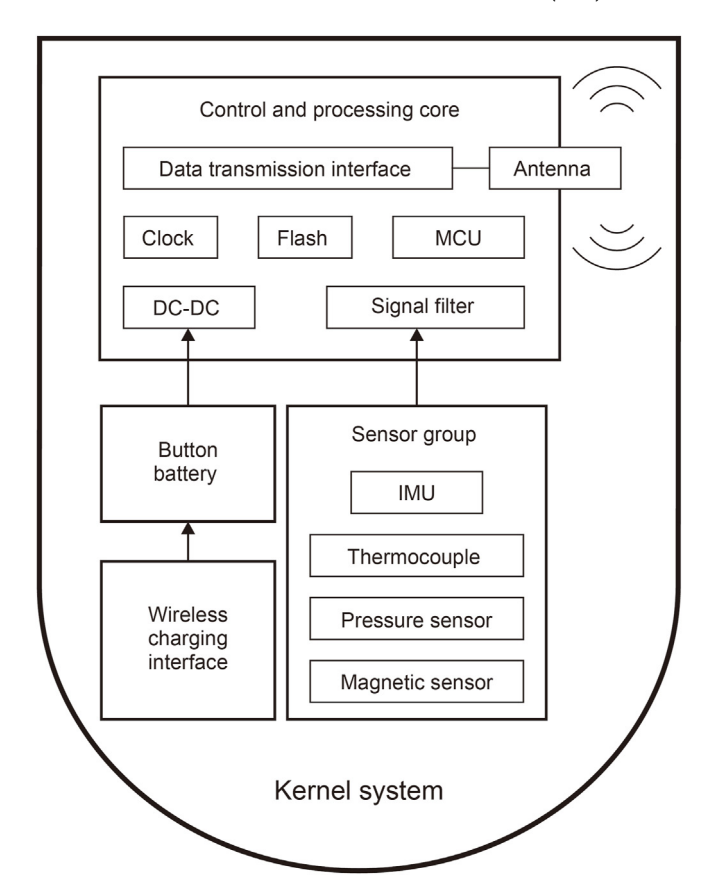


Fig. 1. Schematic of the kernel circuit system.

recovery processes. This study applied the CFD software Fluent to simulate the flow of micro-measurers in four different geometries, aiming to optimize the shape with the best hydrodynamic properties. The four selected geometries include sphere-shaped, bullet-

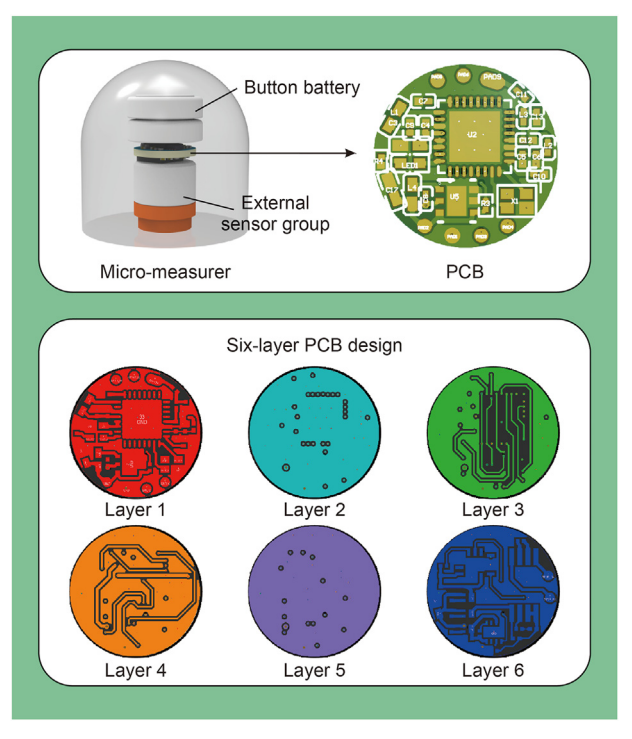


Fig. 2. PCB design of the micro-measurer.

shaped, capsule-shaped, and spindle-shaped, exhibiting sinking and floating motions in the horizontal well fluid domain (this well model has a scale of 1/20000, 0.15 m in length and height). The configuration of the CFD simulation is illustrated in Fig. 3. Transient calculations of the flow field were conducted using the $k-\epsilon$ (kappaepsilon) turbulence model (Launder and Spalding, 1983). The simulation incorporated an overset mesh (Khaware et al., 2018) and a 6 Degrees of Freedom (6-DOF) model to accurately represent the micro-measurer's motion.

The CFD simulation results for the sinking and floating up phases of the micro-measurer are presented in Fig. 4. In the sinking phase, the sphere-shaped exhibits the smoothest trajectory, while the bullet-shaped and spindle-shaped demonstrate the fastest motion speeds. Conversely, during the floating phase, the bullet-shaped not only displays the fastest speed but also the smoothest trajectory. When the bullet-shaped micro-measurer floats up in a simulated 150 mm pipeline, 0.06 s can be saved when compared with other configurations; when an actual 3000 m wellbore is considered, an approximate time savings of 20 min can be obtained. Moreover, as the well depth increases, the time differential between the bullet-shaped design and alternative configurations becomes more pronounced. Consequently, the bullet-shaped has been chosen as designed structure of the micro-measurer.

2.3. Encapsulation via molding

Since the micro-measurer works in the downhole environment, the robust protection from its external protective coatings is necessary. Polydimethylsiloxane (PDMS), a silicon-based organic polymer renowned for its chemical inertness, electrical insulation, thermal stability, and Poisson's ratio approximately 0.5 (Wang et al., 2022; Akhter et al., 2021), imparts the micro-measurer with resilience against downhole temperature, pressure and corrosion. The manufacturing process of the micro-measurer is depicted in Fig. 5. To ensure hermetic sealing, components such as kernel circuits, power supply unit and external sensors are assembled in a bullet-shaped mold, filled with liquid PDMS, and subjected to

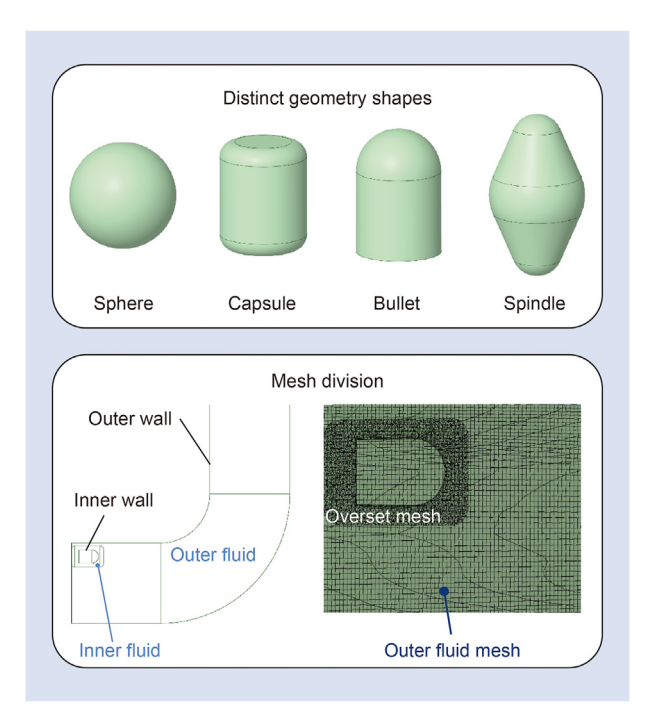


Fig. 3. CFD modeling.

thermal treatment in a high-temperature oven for solidification. In situations of exceptionally high temperatures, the circuit board may be encased in Polytetrafluoroethylene (PTFE) aerogel before molding, thereby enhancing its temperature resistance. The measuring junction of the thermocouple is located at the surface of the micro-measurer, where the environment temperature is tested.

3. Experimental tests

In order to demonstrate the feasibility of micro-measurer, both the laboratory experiments and the field tests were carried out. Specifically, both the stability and the hydrodynamic properties of micro-measurer were tested primarily, and the time-depth conversion methods were investigated experimentally. Subsequently, the micro-measurers were also applied in two exploration wells to measure the downhole temperature and pressure.

3.1. Pressure calibration and experimental verification

To ensure the accuracy of pressure measurement, the calibration of the pressure sensor was carried out on a laboratory hydraulic calibration platform. The confining pressures was set up to 80 MPa with an increment of 10 MPa, the obtained results are depicted in Fig. 6(a). While the temperature sensor was factory-calibrated, and the voltage-temperature correlation was provided by the manufacturer. Subsequently, the reliability of the micro-measurer was testded by experiments conducted in a cold isostatic press and a hightemperature oven, which simulated the downhole high-pressure and high-temperature conditions respectively. The experimental results are shown in Fig. 6(b) and (c), specifically, the pressure applied in cold isostatic press was increased from 0 to 200 MPa with the stepsize of 10 MPa, and the temperature in the oven was increased from 20 to 160 °C with the stepsize 10 °C. During the testing processes, the micro-measurers work stably, and the measured data deviated within 0.5% of the pre-set values, which verified its great measurement accuracy effectively.

3.2. Experimental tests for hydrodynamics of micro-measurer

To assess the hydrodynamic properties of the micro-measurer, a specialized L-shaped experimental setup with a pipe-in-pipe structure and variable diameters, using horizontal wells and extended reach wells as references, was designed and constructed. Illustrated in Fig. 7, the experimental setup measures 3.2 m in length and 3 m in height. Its main body is composed of thickened acrylic material, with the reducer section connected by flanges to ensure both visibility and structural integrity. At the inlet, a ball valve facilitates the dropping of micro-measurers, while the outlet features multiple exits for micro-measurers with diameters ranging from 10 to 24 mm.

Throughout the test, the pre-equipped fluid with its density of 1.13 g/cm³, stored in a reservoir, was continuously pumped into the inner pipe and recirculated back to the reservoir from the outlet. Micro-measurers, with a density of 1.12 g/cm³, were wirelessly controlled and dropped into the inner pipe via the ball valve to initiate circulation. The IMU recorded data characterizing the dynamic behavior of the micro-measurers during circulation. To address high-frequency noise interference in the three-axis acceleration data, Butterworth low-pass filtering was applied for noise reduction. Additionally, to enhance data quality, the three-axis angular velocity data underwent processing using a Kalman filter, which effectively eliminates noise caused by collisions between the micro-measurer and the wall (Welch et al., 1995; Syed et al., 2007). The filtered measurement data is presented in Fig. 8.

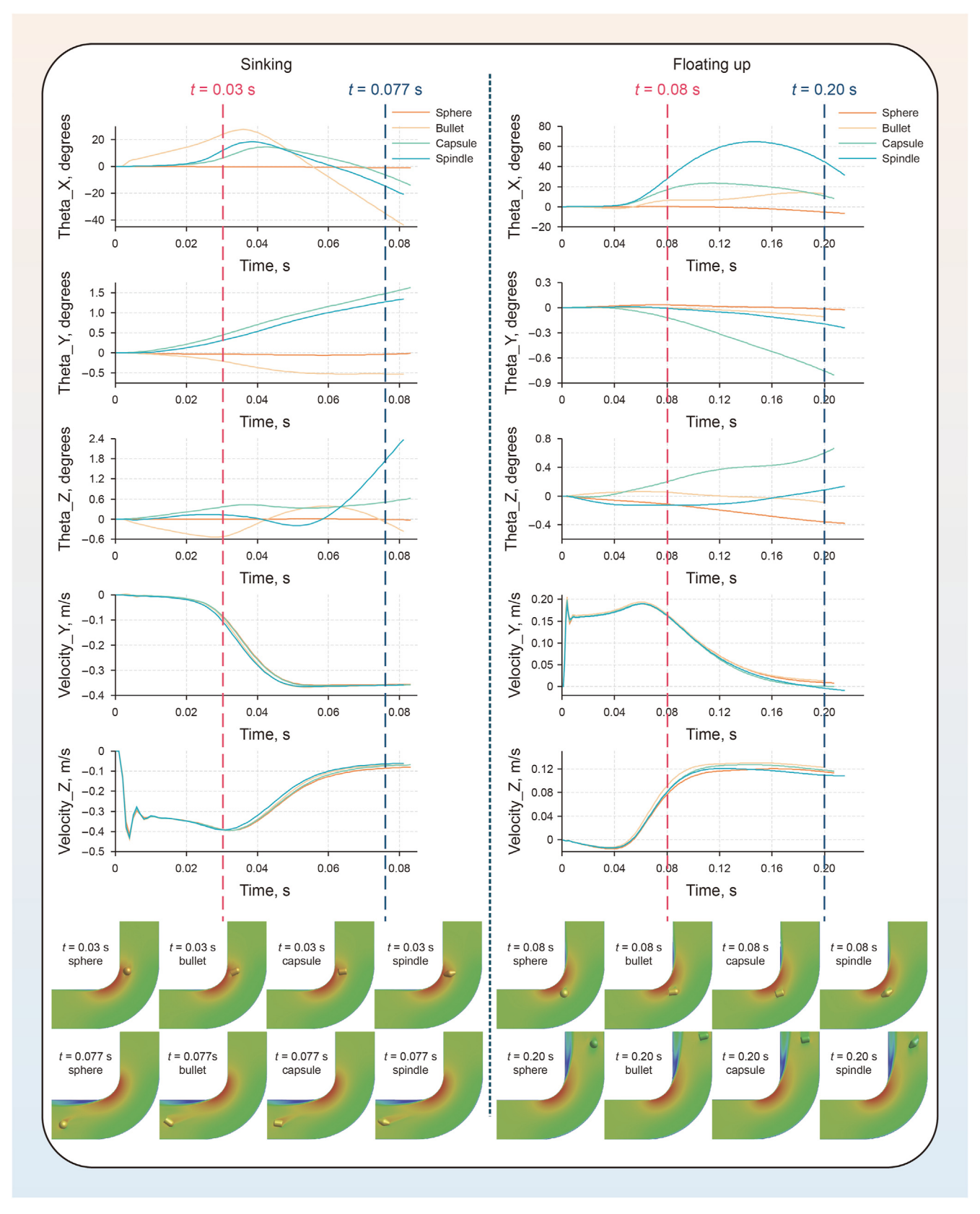


Fig. 4. Results of CFD simulations.

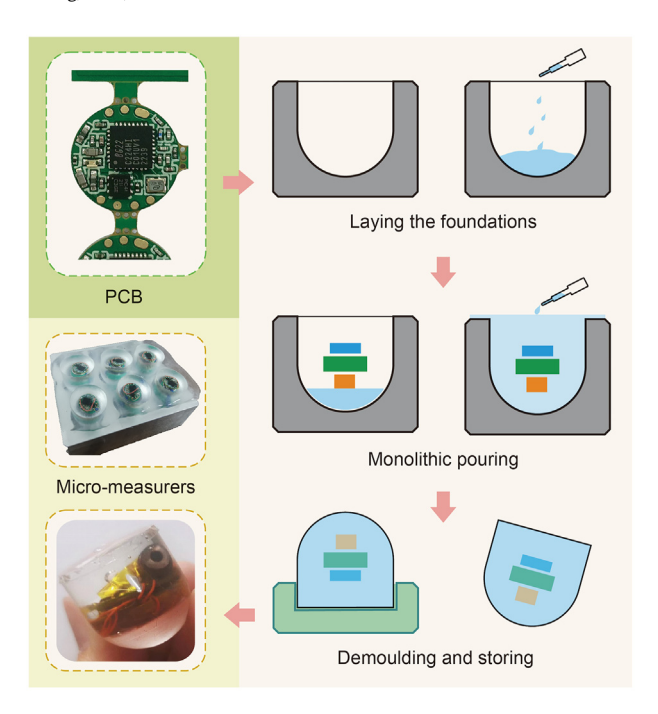


Fig. 5. Encapsulation via molding.

Approximately 27 s after activation, the micro-measurer was released, entering a transient free-fall phase due to a height difference between the ball valve and the liquid surface within the

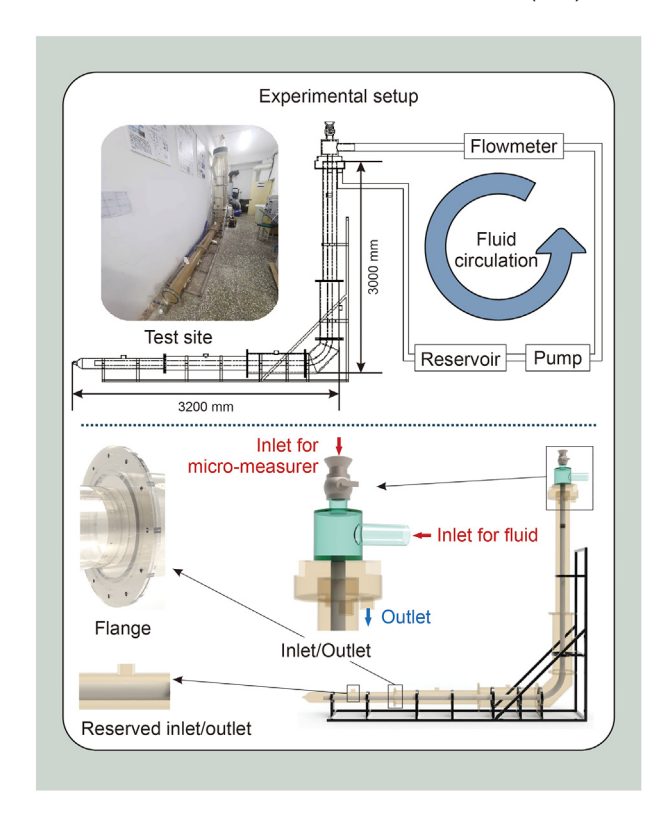


Fig. 7. Schematic of a L-shaped experimental pipe.

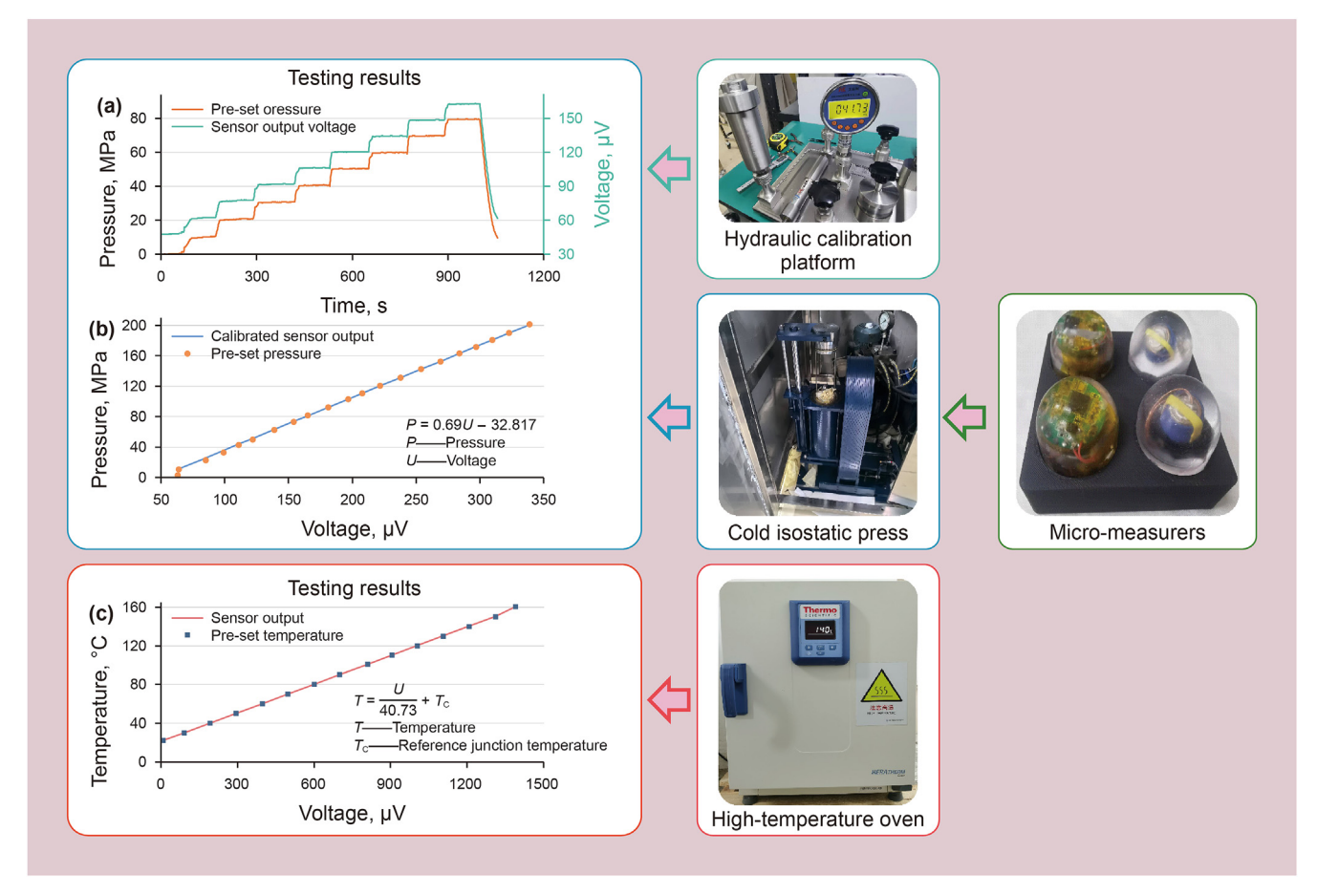


Fig. 6. Pressure calibration and experimental verification.

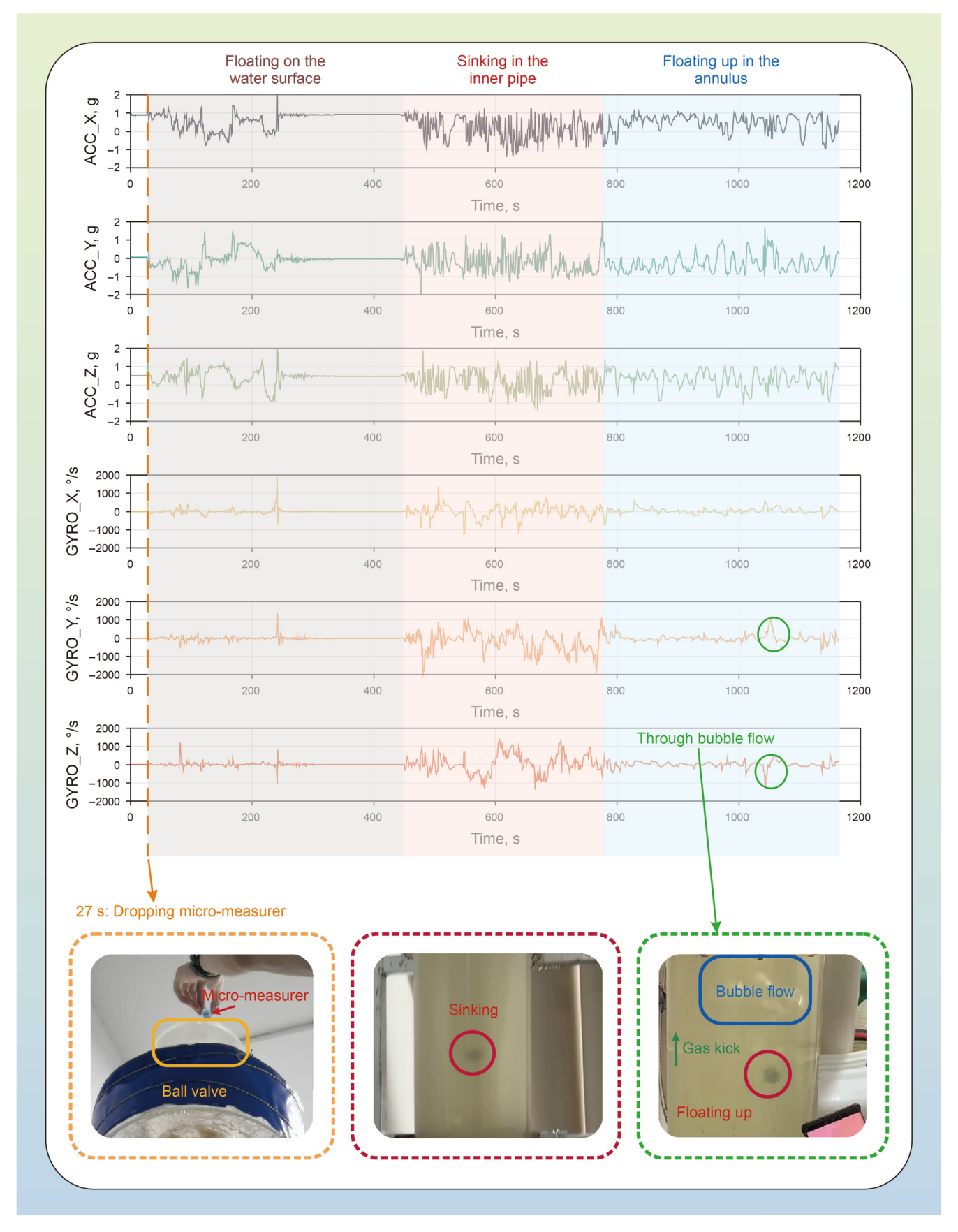


Fig. 8. Measured dynamic signals of the micro-measurer during the hydrodynamic test.

inner pipe. This discrepancy led to a spike in acceleration data. Upon contacting the liquid, the ensuing reaction force caused substantial fluctuations. Subsequently, the micro-measurer floated on the water surface, resulting in acceleration data and angular velocity data remaining near zero. At the 450 s mark, the pump was turned on, initiating the flow of fluid and the movement of the micro-measurer. The direct connection of the inner pipe to the pump resulted in rapid flow velocity and a complex flow state, inducing high amplitude and frequency vibrations of the micro-measurer. By 782 s, as the device entered the annulus, the flow velocity decreased and stabilized, leading to a reduction in vibration amplitude and frequency of the micro-measurer. Ultimately, the micro-measurer successfully returned from the annulus to the reservoir

It is noteworthy that a gas kick condition arising from bubble flow occurred between 1025 and 1038 s. In a vesicular flow environment, the micro-measurer is initially propelled upwards by the flow. Upon encountering the bubble, the micro-measurer experiences a transient free-fall phase due to the absence of fluid support, continuing until it reconnects with the fluid. This results in an instantaneous increase in the amplitude and frequency of acceleration, along with significant changes in angular velocity.

Experimental tests have verified the micro-measurer's stability and resistance for high-temperature and high-pressure downhole conditions and their hydrodynamic properties for moving along the flow of drilling fluid. Through the analysis of the collected dynamic data, the impact of gas kick conditions on the micro-measurer's motion state was initially discerned, which can be further applied for quantitative analysis of gas content in the wellbore.

3.3. Time-depth conversion

3.3.1. Magnetic positioning method

Accurate downhole depth positioning of the micro-measurer can be achieved by installing magnetic rings at identical intervals along the wellbore. The integrated MEMS magnetic sensor of the micro-measurer captures the interval of the peak value of magnetic signal, and this data is utilized for locating the micro-measurer. N magnetic ring markers are fixed at regular intervals δl on the exterior of the drillstring. The value t_0 represents the moment at which the micro-measurer detects the peak value of magnetic signal. The corresponding time point for the entire sinking process are $t_0, t_1, ..., t_n, ..., t_N$, and the depth can be denoted as $n \cdot \delta l$. The equation for the time-depth conversion of the micro-measurer while sinking can be deduced as Eq. (1).

$$L_n = (n-1) \cdot \delta l + \frac{t - t_{n-1}}{t_n - t_{n-1}} \delta l \tag{1}$$

The depth can be calculated in detail by Eq. (2).

$$L_{n} = \begin{cases} \frac{t - t_{0}}{t_{1} - t_{0}} \delta l & t_{0} \leq t < t_{1} \\ 1 \cdot \delta l + \frac{t - t_{1}}{t_{2} - t_{1}} \delta l & t_{1} \leq t < t_{2} \\ \dots & (N - 2) \cdot \delta l + \frac{t - t_{N-2}}{t_{N-1} - t_{N-2}} \delta l & t_{N-2} \leq t < t_{N-1} \\ (N - 1) \cdot \delta l + \frac{t - t_{N-1}}{t_{N} - t_{N-1}} \delta l & t_{N-1} \leq t < t_{N} \end{cases}$$
Similarly, the convenient for the entire flecting

Similarly, the corresponding time points for the entire floating up process are $t_0, t_1, ..., t_n, ..., t_N$, with the depth calculated using the equation:

$$L_{n} = \begin{cases} N \cdot \delta l + \frac{t - t_{0}}{t_{1} - t_{0}} \delta l & t_{0} \leq t < t_{1} \\ (N - 1) \cdot \delta l + \frac{t - t_{1}}{t_{2} - t_{1}} \delta l & t_{1} \leq t < t_{2} \\ \dots & \\ 2 \cdot \delta l + \frac{t - t_{N-2}}{t_{N-1} - t_{N-2}} \delta l & t_{N-2} \leq t < t_{N-1} \\ 1 \cdot \delta l + \frac{t - t_{N-1}}{t_{N} - t_{N-1}} \delta l & t_{N-1} \leq t < t_{N} \end{cases}$$

$$(3)$$

To validate the viability of this approach, six magnetic rings were positioned outside the vertical pipe, with a 1 m gap between each one. Triaxial magnetic field data was recorded by the micromeasurer while sinking and floating. The measured time series data can be subsequently transformed into wellbore depth series using Eqs. (2) and (3). The result as shown in Fig. 9, confirm that the micro-measurer can precisely get the peak value of the magnetic signal when passing through the magnetic ring marker. This method is suitable for the downhole depth positioning of the micro-measurer.

3.3.2. Positioning method using velocity distribution

By examining the forces acting upon the micro-measurer within the drilling fluid, it is possible to calculate the estimated motion

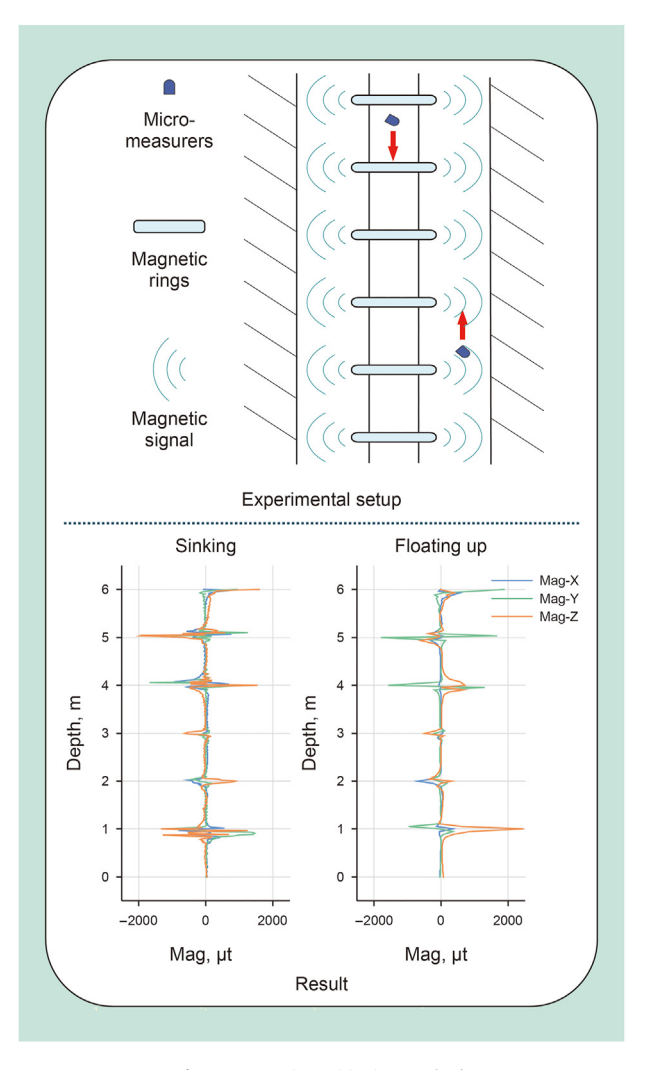


Fig. 9. Magnetic positioning method.

velocity of the micro-measurer in each respective well section, along with the elapsed time for its motion to traverse each well section. Subsequently, the time series data recorded by the micro-measurer can be translated into a corresponding well depth series. The flow velocity of the drilling fluid in each section is determined by the flow rate and cross-sectional area of the drillstring/annulus, as depicted in Eq. (4).

$$v_{\rm f}i = \frac{Q}{A} = \frac{Q}{\frac{\pi}{4} \left(D_i^2 - d_i^2 \right)} \tag{4}$$

where v_i is the flow velocity in well section i, Q is the flow rate, A is the flow area, D_i is the outer diameter of the annulus in well section i (when micro-measurer sinking in the dill string, this parameter represents the inner diameter of the drillstring), and d_i is the inner diameter of the annulus in well section i (this value is 0 when micro-measurer sinking).

The micro-measurer is influenced by the combined effects of gravity F_g , buoyancy F_b , and drag F_D in the fluid. The three factors can be described by Eq. (5):

$$\begin{cases}
F_{g} = m_{b}g \\
F_{b} = \rho g V_{b}
\end{cases}$$

$$F_{D} = C_{D} \rho A_{b} \frac{1}{2} \left| v_{f} - v_{b} \right| \left(v_{f} - v_{b} \right)$$
(5)

where m_b , V_b , A_b and v_b are the mass, volume, flow area, and motion velocity of the micro-measurer, ρ and v_f are the density and flow velocity of the drilling fluid, respectively. C_D represents the drag coefficient.

When the micro-measurer is in a state of uniform speed, the relationship between gravity, buoyancy, and drag can be simplified as:

$$F_{\rm g} - F_{\rm b} - F_{\rm D} = 0 \tag{6}$$

$$m_{\mathbf{b}}g - \rho gV_{\mathbf{b}} - C_{\mathbf{D}}\rho A_{\mathbf{b}} \frac{1}{2} \left| v_{\mathbf{f}} - v_{\mathbf{b}} \right| \left(v_{\mathbf{f}} - v_{\mathbf{b}} \right) = 0 \tag{7}$$

where C_D is the drag coefficient between the micro-measurer and the drilling fluid, which is determined by the Reynolds number:

$$Re = \frac{d_{\rm b} \left| v_{\rm f} - v_{\rm b} \right| \rho}{\mu} \tag{8}$$

Here, μ means the viscosity of the drilling fluid, and $d_{\rm b}$ is diameter of the micro-measurer.

For the past few years, numerous fluid flow experiments have been conducted, leading to the proposal of three models for estimating the drag coefficient as shown in Eq. (9) (He et al., 2014; Zhang et al., 2016):

$$C_{\rm D} = \begin{cases} \frac{34}{Re^{0.625}} \\ \frac{30}{Re} + \frac{67.289}{e^{5.030\psi}} \\ \frac{24}{Re} \left(1 + 0.173Re^{0.657} \right) + \frac{0.413}{1 + 16300Re^{-1.09}} \end{cases}$$
(9)

where ψ represents the spherical coefficient of the micro-measurer, with ball $\psi = 1$, capsule $\psi = 0.8$, and bullet $\psi = 0.82$. Eqs. (7)–(9)

enable the computation of v_{bi} (v_b in well section i). Consequently, the downhole depth position s of the micro-measurer at any given time T_i can be calculated as Eq. (10):

ined ulus,
$$(4) \qquad s = \begin{cases} v_{b1}T_i & 0 < T_i \le \frac{h_1}{v_{b1}} \\ h_1 + v_{b2} & \left(T_i - \frac{h_1}{v_{b1}}\right) \frac{h_1}{v_{b1}} < T_i \le \frac{h_1}{v_{b1}} + \frac{h_2}{v_{b2}} \\ h_1 + h_2 + \dots + v_{bn} \left(T_i - \frac{h_1}{v_{b1}} - \dots - \frac{h_{n-1}}{v_{bn-1}}\right) \\ \frac{h_1}{v_{b1}} + \dots + \frac{h_{n-1}}{v_{bn-1}} < T_i \le \frac{h_1}{v_{b1}} + \dots + \frac{h_n}{v_{bn}} \end{cases}$$

$$(10)$$

4. Field test

4.1. Field test in #Yantan-1

To validate the micro-measurer's functions during actual downhole operations, a field test was conducted at #Yantan-1 (site in Chongqing Municipality, China). #Yantan-1 is an exploration well designed to reach a depth of 6779 m, and the field test was conducted at a depth of 502 m. During the test, the outer diameter of drillstring was 65 mm, the wellbore casing's diameter was 165 mm, the nozzle of the drill bit measured 33 mm, and the drilling mud was water-based, with its density of 1.15 g/cm³ and plastic viscosity of 36 mPa·s.

Throughout the test, 14 micro-measurers with a density of 1.12 g/cm³ were dropped into the drillstring for circulation, and 6 of them were successfully recovered at the vibrating screen, achieving a 42.8% recovery success rate. All recovered micro-measurers recorded complete data. Fig. 10 illustrates the testing process.

The tested micro-measurers were wireless activated and set a sampling frequency of 1 Hz. They recorded both the wellbore's temperature and their own acceleration and angular velocity during the circulation. Fig. 11 shows the data recorded by one of the recovered micro-measurers. Data processing enabled analysis of the micro-measurers' sinking, vibrating, and floating up motion in downhole environment. The rise in measured temperature data was observed after the pump was turned on, and micro-measurers began sinking in the drillstring, demonstrating the measurement capability of the micro-measurer.

To construct the wellbore temperature profile, the positioning method using velocity distribution is applied to process the measured data, combined with the calibration of micro-measurers' motion phase based on the recorded dynamic signals, as shown in Fig. 12. The annulus exhibits a higher temperature as it is closer to the formation. Considering the absence of significant pressure changes in the wellbore, the pressure measurement module was not installed in this test.

Following the field test in #Yantan-1, although the limited experience resulted in a less than ideal recovery rate, it was proved that the micro-measurer can obtain downhole physical parameters, circulate back with drilling fluid, and construct a temperature profile using the time-depth conversion method.

4.2. Field test in #Qingqianping-101

The field test conducted at #Qingqianping-101 (site in Sichuan Province, China) was an application of the micro-measurer in pressure coring. To supply for the measurement of over 20 h in

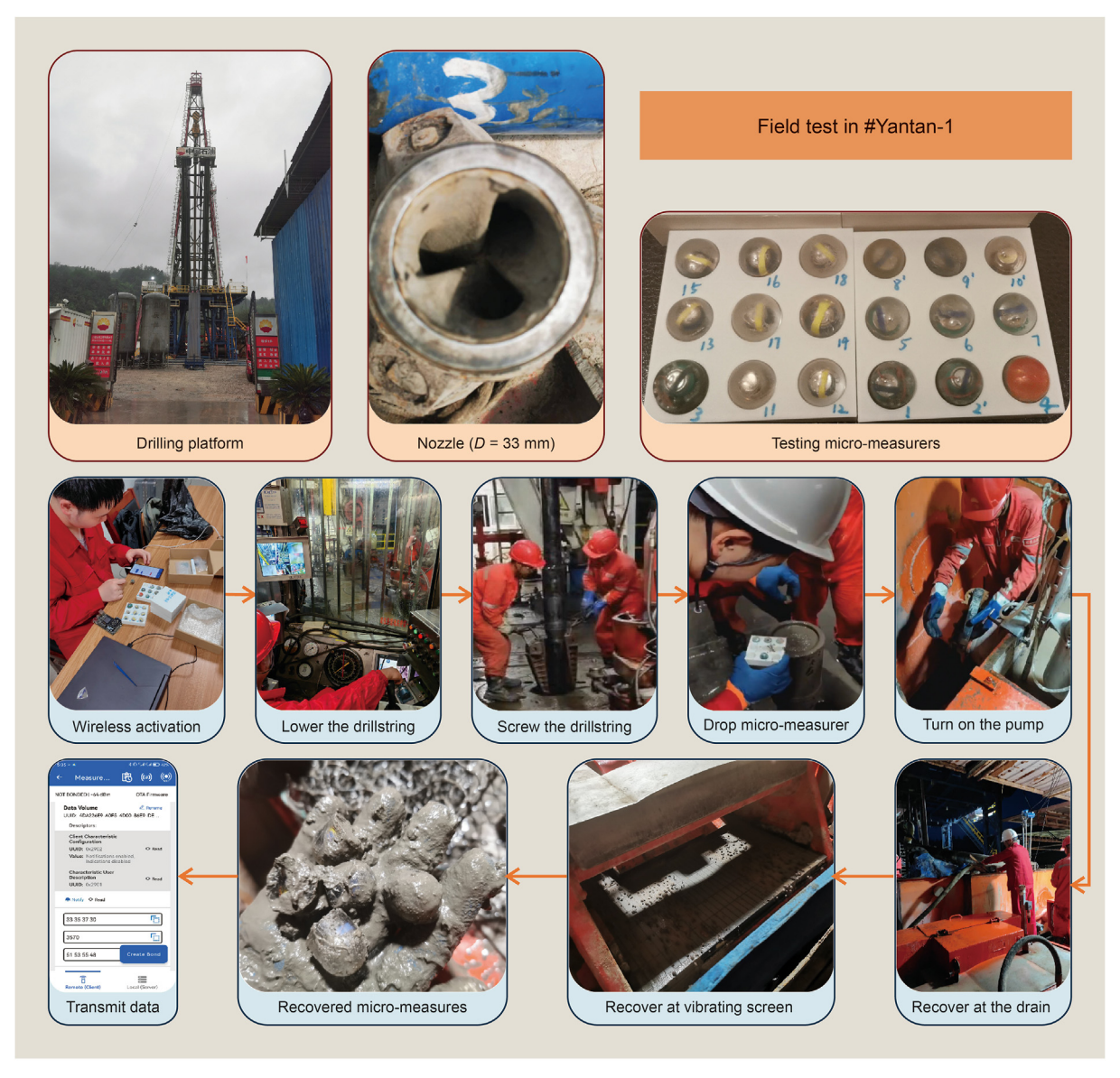


Fig. 10. Process of field test in #Yantan-1.

pressure coring work, testing micro-measurers were wireless activated and set a sampling frequency of 1/120 Hz, deployed in the pressure core barrel, and lowered to 1049 m depth, finally recovered when the coring finished and drillstring lifted, the testing process and results are shown in Fig. 13.

At 2 h and 18 min, the drill string was lowered, measured temperature and pressure began rising. At 4 h and 42 min, pressure coring began, pressure in the barrel was maintained at over 10 MPa until the removal of core at 22 h and 38 min, pressure suddenly dropped from the standard of over 10 MPa to the normal condition due to the barrel pressure relieved.

Measured pressure and temperature data in #Qingqianping-101 are consistent with the operation situation, confirms the measuring function of the pressure sensor and the feasibility of micromeasurer, can be applied as a real-time measurement tool of pressure and temperature in pressure coring.

5. Downhole intelligent joint for releasing micro-measurers

In order to avoid the limitation of nozzle of drill bit on the size of the micro-measurer, a downhole intelligent joint for releasing micro-measurers at bottomhole was considered. Moreover, such an intelligent joint can be further applied as a downhole terminal to be a part of a downhole IoT system.

5.1. Design of intelligent joint

The intelligent joint releases the micro-measurer directly into the annulus, thereby eliminating size constraints and risk of damage of micro-measurer when flowing out the nozzle. Three methods for releasing the micro-measurer are offered in this research: directly dropping into the drillstring or releasing to the annulus using the two different controllable releasing structures of intelligent joint, as illustrated in Fig. 14. The designed releasing structures include a mechanical system and an inductive electric system. 3D printed prototypes from polylactide material are produced to evaluate these designs, as illustrated in Fig. 15.

5.1.1. Intelligent joint with mechanical driving system

The mechanical intelligent joint facilitates control of the releasing process by utilizing a steel ball for pressure build-up

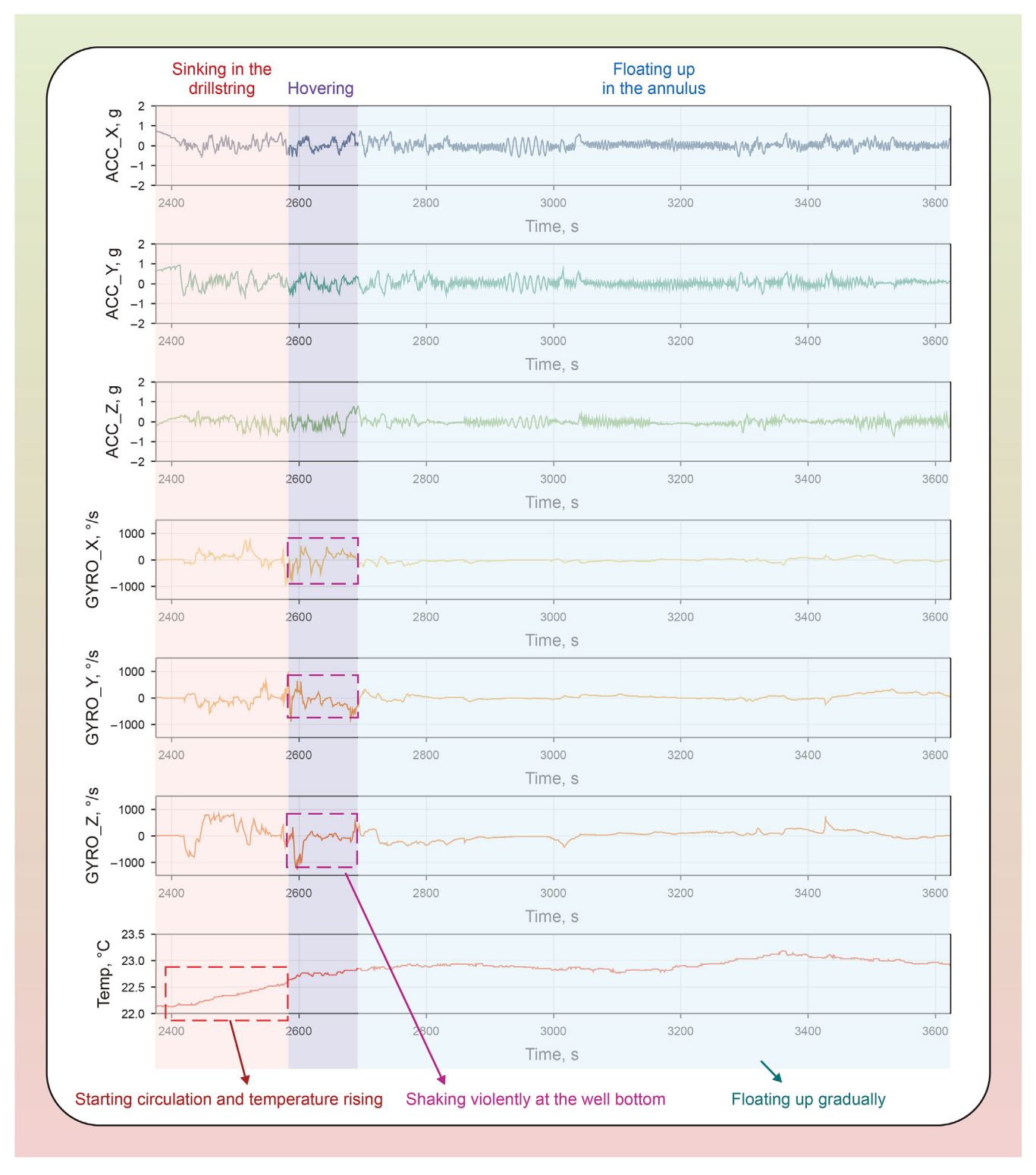


Fig. 11. Measured signals for field test in #Yantan-1.

and a pin-slot reversal mechanism for motion transformation. The longitudinal displacement caused by the steel ball is converted into circumferential rotation, leading to the release of the micro-measurer from the cabin. The mechanical intelligent joint consists of three main parts: the driving mechanism, reversing mechanism, and releasing mechanism, as depicted in Fig. 15.

The driving mechanism consists of a release pin and a piston body. When the steel ball drops, it contacts multiple release pins, obstructing the flow of drilling fluid and building up pressure. This pressure drives the release pin and the piston body downwards. Upon reaching the cylinder cone's slope, the steel ball is released, relieving the pressure, and the reaction force from the spring initiating a reset. The core of the reversing mechanism is a pin-slot

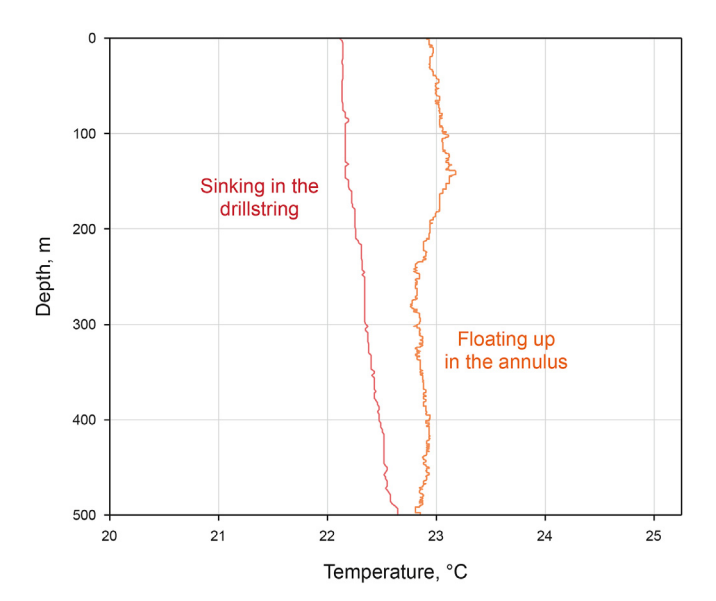


Fig. 12. Temperature profile via time-depth conversion.

reversing device. The longitudinal movement of the piston body causes the connected rotating pins to undergo circumferential rotation through the slope and spiral slot. The releasing mechanism, comprising several cabins and ratchets, facilitates the release of the micro-measurer in the cabin through the movement of the rotating body. Ratchets can limit position and prevent reversal.

5.1.2. Intelligent joint with inductive electric driving system

Radio Frequency Identification (RFID) provides an alternative for releasing control, potentially simplifying the structure of the intelligent joint. In this implementation, the ball released from the drillstring no longer serves to build up pressure but incorporates an RFID tag for transmitting commands to the RF module of the intelligent joint. In this configuration, the intelligent joint is composed of two main components: the driving mechanism and the reversing mechanism, as depicted in Fig. 15.

The driving mechanism comprises a RF module and a brushless motor. Upon recognizing the RFID tag ball, the industrial personal computer controls the motor's rotation based on the content. The releasing mechanism follows the same structure as the mechanical system scheme.

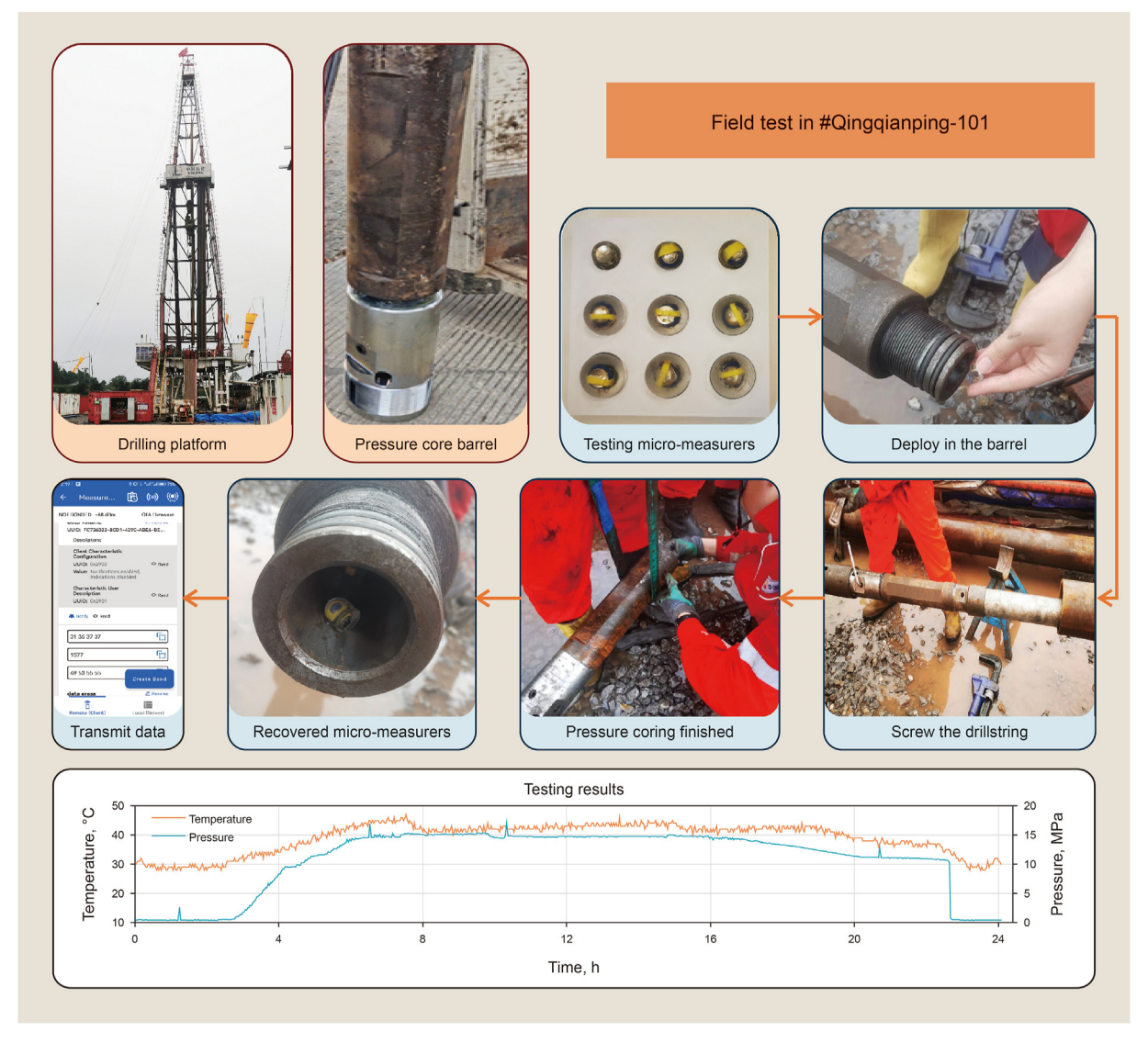


Fig. 13. Process and results for field test in #Qingqianping-101.

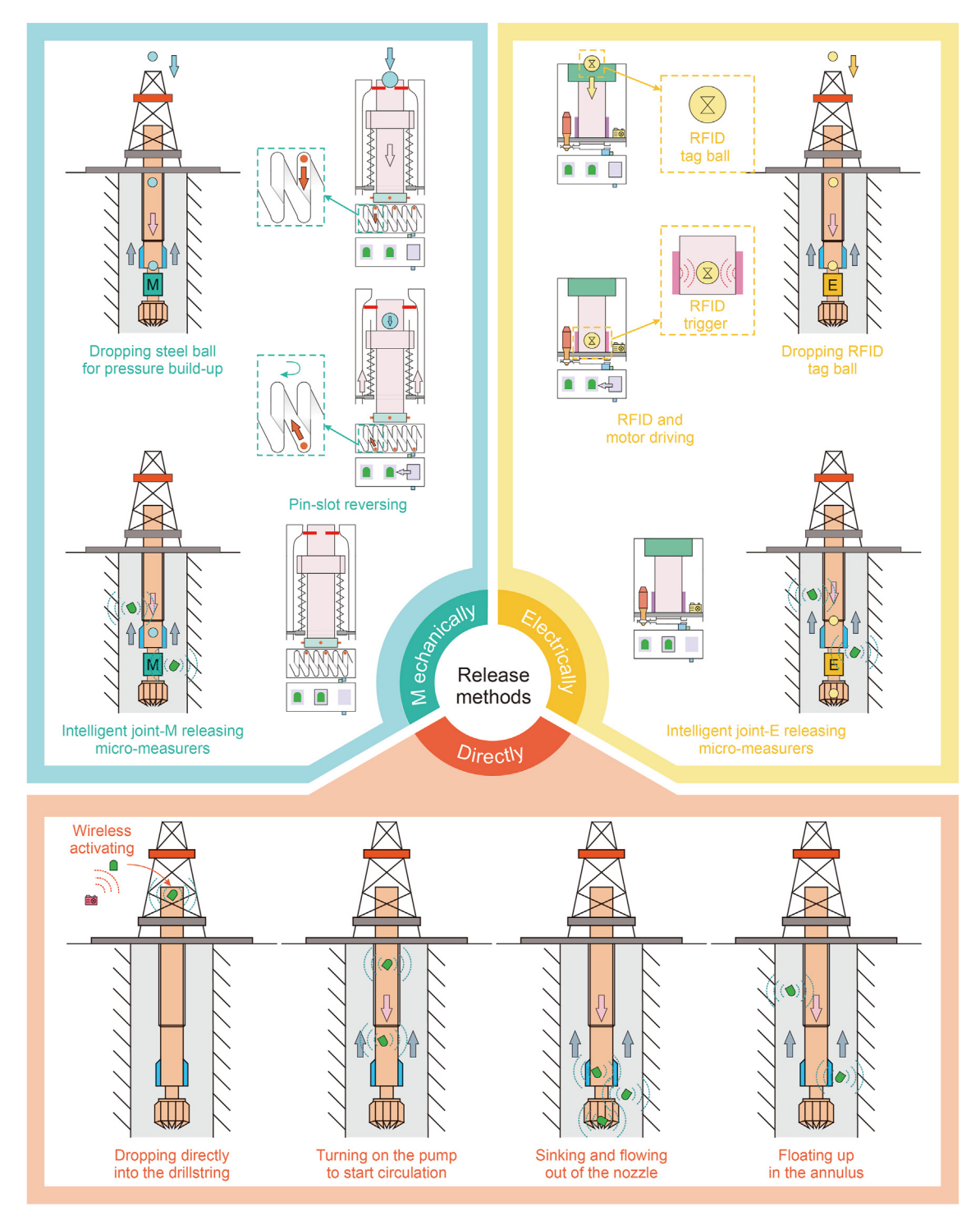


Fig. 14. Three kinds of release methods for the micro-measurer.

5.2. Downhole IoT based on micro-measurers and intelligent joints

As the future work, the information exchange mode between multiple micro-robots and the intelligent releasing joints will be explored, based on which, an information collaboration mechanism for a local bottomhole closed-loop can be developed; and ultimately a downhole IoT system can thus be built, as illustrated in Fig. 16. The development of downhole IoT system will be divided into three stages.

In the initial stage, the structural design of the intelligent joint undergoes iterative updates, and a fast identification method for

wireless radio frequency signals will be established for high-speed flowing environments, and thus to make the downhole intelligent joint achieve controllable release of micro-robots in the wellbore annulus. This advancement allows for a larger size of the micro-measurer, incorporating additional MEMS devices and even actuators.

In the subsequent stage, the intelligent joint will integrate an intelligent industrial personal computer with high-precision sensors. Therefore, it can serve as a downhole intelligent terminal which can transmit significant historical data into micro-measurers



Fig. 15. Structural design of the intelligent joint.



Fig. 16. Downhole IoT system based on micro-measurers and intelligent joint.

before their releasing. Moreover, it can also automatically control the releasing frequency of micro-measurers based on analysis of the real downhole condition.

In the final stage, the intelligent joint can receive variety of data from downhole measurement tools, and communicate with the micro-measurers around it, to build a local control closed-loop to solve downhole complexities.

6. Conclusions

This research outlines the development, verification, and application of a new generation of micro-measurers which can moving with drilling fluid, measuring downhole multiple physical parameters, and constructing wellbore temperature/pressure

profiles via correlating the measured time series data with the drilling depth.

According to the experimental tests for hydrodynamics of micro-measurer, the six-axis IMU can effectively detect the vibration conditions of micro-measurers based on obvious variations of both the vibration amplitude and frequency of the micro-measurer in different downhole multiphase flow circumstances, which can be further applied for quantitative analysis of gas content in the wellbore.

Two field tests have proved the feasibility and reliability of the micro-measurers. In #Yantan-1, micro-measurers achieved a 42.8% recovery rate for downhole temperature measurements, and constructed wellbore temperature profile using time-depth conversion method based on velocity distribution. In #Qingqianping-101, both the downhole temperature and pressure conditions have been measured successfully by using the micro-measurers.

As the future work, the information exchange mode between multiple micro-robots and the intelligent releasing joints will be explored to develop a local control loop; and thus an Internet of Things system can be built for monitoring downhole complexities. By this way, a new solution for "measurement-transmission-control" technology for intelligent drilling engineering can thus be expected.

CRediT authorship contribution statement

Yu-Xi Wang: Writing — original draft, Software, Methodology. **Mu Li:** Resources, Project administration, Investigation, Funding acquisition, Conceptualization. **Mao-Lin Liao:** Writing — review & editing, Validation, Project administration, Methodology,

Investigation, Conceptualization. **Wei Liu:** Investigation, Formal analysis, Conceptualization. **Ting-Rui Li:** Visualization, Formal analysis. **Joseph Páez Chávez:** Writing — review & editing. **Gong-Hui Liu:** Conceptualization. **Jun Li:** Conceptualization. **Sheng-Lian Yao:** Formal analysis.

Data availability

The datasets generated and analysed during the current study are available from the corresponding author on reasonable request.

Declaration of competing interest

The authors declare that they have no known competing financial interests or personal relationships that could have appeared to influence the work reported in this paper.

Acknowledgement

This paper was supported by the National Natural Science Foundation of China (No. U22B2072), and the Research Project of China Petroleum Science and Technology Innovation Fund (No. 2025DQ02-0144).

References

- Akhter, F., Siddiquei, H., Alahi, M.E.E., Mukhopadhyay, S.C., 2021. An iot-enabled portable sensing system with mwcnts/pdms sensor for nitrate detection in water. Measurement 178, 109424. https://doi.org/10.1016/j.measurement.2021.109424.
- An, J., Li, J., Huang, H., Liu, G., Yang, H., Zhang, G., Li, W., 2023. Mud loss behavior in fractured formation with high temperature and pressure. Energy Rep. 9, 2638–2652. https://doi.org/10.1016/j.egyr.2023.01.080.
- Dokhani, V., Li, B., Gooneratne, C., Zhan, G., Moellendick, T.E., Shi, Z., 2022. Evaluation of circulating temperature in wellbores using drilling microchips: modeling and case studies. J. Petrol. Sci. Eng. 211, 110129. https://doi.org/10.1016/j.petrol.2022.110129.
- Emmerich, W., Akimov, O., Brahim, I.B., Greten, A., 2015. Reliable high-speed mud pulse telemetry. In: SPE/IADC Drilling Conference and Exhibition. OnePetro. https://doi.org/10.2118/173032-MS.
- Gurjao, K.G.R., Gildin, E., Gibson, R., Everett, M., 2021. Modeling of distributed strain sensing (dss) and distributed acoustic sensing (das) incorporating hydraulic and natural fractures interaction. In: Unconventional Resources Technology Conference, pp. 3568–3587. https://doi.org/10.15530/urtec-2021-5414.
- Gutierrez, D., Anderson, N., Hanak, C., Paton, T., Vallejos, J., Brown, N., 2021. Realtime wellbore placement improvement with high-fidelity trajectory estimation and dual-sensor mwd packages. In: SPE Annual Technical Conference and Exhibition. https://doi.org/10.2118/206253-MS.
- Hancke, G.P., Silva, B.J., 2021. Wireless positioning in underground mines: challenges and recent advances. IEEE Indust. Electron. Magaz. 15, 39–48. https://doi.org/10.1109/MIE.2020.3036622.
- He, M., Liu, G., Li, J., Li, M., Wang, H., 2014. The research of cuttings migration during gas invasion. Sci. Technol. Eng. 27—31.
- He, X., Xie, S., Gu, L., Liu, F., Zhang, M., Lu, H., 2022. High-resolution quasidistributed temperature and pressure sensing system for deep-sea reservoir monitoring. Measurement 199, 111568. https://doi.org/10.1016/j.measurement. 2022.111568.
- Hemink, G., van der Horst, J., 2018. On the use of distributed temperature sensing and distributed acoustic sensing for the application of gas lift surveillance. SPE Prod. Oper. 33, 896–912. https://doi.org/10.2118/191130-PA.
- Khaware, A., Srikanth, K., Gupta, V.K., 2018. Numerical simulation of free surface flows using overset mesh. In: Offshore Technology Conference Asia. https:// doi.org/10.4043/28461-MS.
- Launder, B.E., Spalding, D.B., 1983. The numerical computation of turbulent flows. In: Numerical Prediction of Flow, Heat Transfer, Turbulence and Combustion. Elsevier, pp. 96–116. https://doi.org/10.1016/B978-0-08-030937-8.50016-7.
- Li, B., Dokhani, V., Zhan, G.D., Sehsah, O., 2020. Evaluating distribution of circulating temperature in wellbores using drilling microchips. In: Abu Dhabi International Petroleum Exhibition & Conference. OnePetro. https://doi.org/10.2118/203170-MS

- Li, B., Gooneratne, C.P., Badran, M.S., Shi, Z., 2017. Implementation of a drilling microchip for downhole data acquisition. In: SPE/IATMI Asia Pacific Oil & Gas Conference and Exhibition. OnePetro. https://doi.org/10.2118/186330-MS
- Li, M., Liu, W., Zhang, H., Tang, C., Fu, J., Zhai, X., Wang, H., 2023a. Field test research on the downhole multiphysics micro-measurer based on the mems microchip. Front. Earth Sci. 11, 1164839. https://doi.org/10.3389/feart.2023.1164839.
- Li, P., Wang, L., Zu, Y., Bai, X., Hu, Y., 2023b. Multi-sensor fusion method based on ffrfk for 3d trajectory measurement of underground pipelines. Tunn. Undergr. Space Technol. 141, 105344. https://doi.org/10.1016/j.tust.2023.105344.
- Li, S., Gao, R., Li, J., Zhu, Z., Wang, Z., Gramajo Silva, E.D., 2022. Study and Implement of the Large Amount Data Divided Time Transmission System Utilizing Microchip-Storage-Ball Release while Drilling. In: International Petroleum Technology Conference. https://doi.org/10.2523/IPTC-22368-MS
- Liu, H.F., Luo, Z.C., Hu, Z.K., Yang, S.Q., Tu, L.C., Zhou, Z.B., Kraft, M., 2022. A review of high-performance mems sensors for resource exploration and geophysical applications. Pet. Sci. 19, 2631–2648. https://doi.org/10.1016/j.petsci.2022. 06.005
- Liu, W., Liao, M., Li, M., Zhu, Z., Fu, J., 2023. A downhole multiphysics measuring device based on mems microchips. J. China Univer. Petrol. 47, 87–95. https://doi.org/10.3969/j.issn.1673-5005.2023.03.010.
- van Pol, A., van Pol, J., McNealy, R., Goudy, C., 2018. The future of in-line inspection: free-floating smart sensors. In: International Pipeline Conference. American Society of Mechanical Engineers. https://doi.org/10.1115/IPC2018-78662.
- Shi, Z., Li, B., Gooneratne, C., Zhan, G.D., 2020. Wireless activated drilling microchip for wellbore temperature measurement. In: International Petroleum Technology Conference. https://doi.org/10.2523/IPTC-19985-MS.
- Sun, Y., Xue, Z., Hashimoto, T., Zhang, Y., 2021. Optically quantifying spatiotemporal responses of water injection-induced strain via downhole distributed fiber optics sensing. Fuel 283, 118948. https://doi.org/10.1016/j.fuel.2020.118948.
- Suo, Y., Zhao, Y.J., Fu, X.F., He, W.Y., Pan, Z.J., 2023. Mixed-mode fracture behavior in deep shale reservoirs under different loading rates and temperatures. Pet. Sci. 20, 3037–3047. https://doi.org/10.1016/j.petsci.2023.05.009.
- 20, 3037—3047. https://doi.org/10.1016/j.petsci.2023.05.009.

 Syed, Z.F., Aggarwal, P., Goodall, C., Niu, X., El-Sheimy, N., 2007. A new multiposition calibration method for mems inertial navigation systems. Meas. Sci. Technol. 18, 1897. https://doi.org/10.1088/0957-0233/18/7/016.
- Wang, B., Li, J., Zhang, G., Li, Y., Huang, H., Zhan, J., Yang, H., 2023. A novel early gas kick monitoring method using the difference between downhole dual measurement points pressure and a genetic algorithm-based model. Geoenergy Sci. Eng. 231, 212371. https://doi.org/10.1016/j.geoen.2023.212371.
- Wang, C., Liu, G., Yang, Z., Li, J., Zhang, T., Jiang, H., He, M., Luo, M., Li, W., 2020. Downhole gas-kick transient simulation and detection with downhole dual-measurement points in water-based drilling fluid. J. Nat. Gas Sci. Eng. 84, 103678. https://doi.org/10.1016/j.jngse.2020.103678.
- Wang, L., Noureldin, A., Iqbal, U., Osman, A.M., 2018. A reduced inertial sensor system based on mems for wellbore continuous surveying while horizontal drilling. IEEE Sens. J. 18, 5662–5673. https://doi.org/10.1109/JSEN.2018.28 40162
- Wang, M., Zhang, Y., Bin, J., Niu, L., Zhang, J., Liu, L., Wang, A., Tao, J., Liang, J., Zhang, L., et al., 2022. Cold laser micro-machining of pdms as an encapsulation layer for soft implantable neural interface. Micromachines 13, 1484. https://doi.org/10.3390/mi13091484.
- Welch, G., Bishop, G., et al., 1995. An Introduction to the Kalman Filter.
- Yan, Z., Xu, W., Ai, C., Geng, Y., 2019. Parametric study on pump noise processing method of continuous wave mud pulse signal based on dual-sensor. J. Petrol. Sci. Eng. 178, 987–998. https://doi.org/10.1016/j.petrol.2019.04.018.
- Yu, M., He, S., Chen, Y., Takach, N., LoPresti, P., Zhou, S., Al-Khanferi, N., 2012. A distributed microchip system for subsurface measurement. In: SPE Annual Technical Conference and Exhibition. OnePetro. https://doi.org/10.2118/ 159583-MS.
- Zhang, H., Li, G., Xiao, L., Yang, C., 2016. Study on the influence of the rotation of drill string on cuttings transportation in horizontal well. Sci. Technol. Eng. 16, 125–130. https://doi.org/10.3969/j.issn.1671-1815.2016.02.025.
- Zhang, K., Liu, X.F., Wang, D.B., Zheng, B., Chen, T.H., Wang, Q., Bai, H., Yao, E.D., Zhou, F.J., 2024. A review of reservoir damage during hydraulic fracturing of deep and ultra-deep reservoirs. Pet. Sci. 21, 384–409. https://doi.org/10.1016/ i.petsci.2023.11.017.
- Zhang, Z., Sun, B., Wang, Z., Pan, S., Lou, W., Sun, D., 2023. Early monitoring method of downhole accident driven by physics based model and data driven methods coupling. Geoenergy Sci. Eng. 221, 111296. https://doi.org/10.1016/j.petrol.20 22 111296
- Zhu, Z., Zhao, J., Mulunjkar, A., Rached, R., Gramajo, E., Li, F., Wang, Z., Shi, Z., Zhang, W., Zhao, W., 2021. Measurements during drilling through an innovative microchip technology to determine accurate wellbore properties for efficient drilling operations. In: SPE Annual Technical Conference and Exhibition. https://doi.org/10.2118/205899-MS.